Thermochimica Acta, 216 (1993) 45–79
Elsevier Science Publishers B.V., Amsterdam

Estimates for the enthalpy of formation of rare-earth oxyhalides with the P4/*nmm* structure

C.W. Struck and J.A. Baglio
GTE Laboratories, 40 Sylvan Road, Waltham, MA 02254 (USA)

(Received 12 June 1992)

Abstract

The enthalpies of formation of the rare-earth oxyhalides that have the P4/*nmm* (PbFCl) structure are estimated through the energy of formation W_t of the species from the gaseous ions. These estimates afford reasonable values for the energies of dissociation into oxide and halide phases. However, to obtain agreement with lattice energy calculations using the Busing potential energy function and lattice sum computer program, we were forced to abandon the assumption that the van der Waals and the repulsive energy parameters in this potential energy were unique for each type of ion. Rather, we required variabilities in these parameters for the oxide and for the halides across the rare-earth series and for the metal ions from halide to halide. The number of such parameters to be found increased from 54 to 405. To restore uniqueness, we chose to invoke the criterion of smooth behavior from species to species, in crystallographic parameters, in the repulsive and van der Waals parameters, in the total energy and its components, and in the individual bond energies and their components. A unique set of crystallographic parameters and Busing parameters was found for all oxyhalide phases which gave the values for W_t as estimated, and which essentially satisfied the smoothness criterion. The criterion of smoothness leads to lattice descriptions somewhat different from published crystallographic data, particularly for the oxybromides.

INTRODUCTION

Motivation

Rare earth oxyhalides are important in the lamp chemistry of new rare-earth-containing lamp fills. From among the halides, the triiodides are used because they are least reactive with the quartz or alumina lamp envelope and with the tungsten electrodes. A cause of the degradation of these lamps is the slow reaction of the lamp fill with the lamp envelope materials, which renders the rare-earth involatile. The oxyiodides are

Correspondence to: C.W. Struck, GTE Laboratories, 40 Sylvan Road, Waltham, MA 02254, USA.

0040-6031/93/$06.00 © 1993 – Elsevier Science Publishers B.V. All rights reserved

TABLE 1

W_t, its components, and derived $\Delta H^{\ominus}_{f,298}$

M	X	W_t	W_c	W_v	W_r	$\Delta H^{\ominus}_{f,298}$		W_t (lit.)	Ref.
						This work	Lit.		
La	Cl	−1325.9	−1516.6	−241.9	432.5	−236.9	−241.6	−1330.6	10
							−244.8	−1333.8	12
Ce	Cl	−1340.7	−1530.3	−268.5	458.2	−235.9	−239.0	−1343.8	10
Pr	Cl	−1350.4	−1548.8	−305.1	503.5	−237.5	−242.0	−1354.9	10
Nd	Cl	−1360.1	−1560.4	−328.6	528.9	−237.3	−239.0	−1361.8	10
Pm	Cl	−1369.4	−1567.9	−346.4	544.9	−249.5			
Sm	Cl	−1377.3	−1575.8	−366.8	565.3	−239.1	−237.1	−1375.3	10
Eu	Cl	−1385.9	−1583.0	−386.6	583.7	−219.3			
Gd	Cl	−1393.7	−1589.6	−404.4	600.3	−242.3	−234.0	−1385.4	10
Tb	Cl	−1399.8	−1595.3	−421.5	617.0	−240.7	−233.0	−1392.1	10
							−234.0	−1393.1	11
Dy	Cl	−1406.7	−1602.2	−435.9	631.4	−243.1	−235.9	−1399.5	10
Ho	Cl	−1413.7	−1601.4	−444.7	632.5	−244.1	−239.2	−1408.8	10
Er	Cl	−1419.5	−1609.1	−460.9	650.5	−243.3	−237.9	−1414.1	10
Tm	Cl	−1424.4	−1617.6	−476.1	669.3	−241.4	−236.0	−1419.0	10
Yb	Cl	−1427.5	−1625.1	−486.9	684.5	−224.8	−229.9	−1432.6	10
Lu	Cl	−1430.4	−1632.5	−497.8	700.0	−239.1	−227.1	−1418.4	10
La	Br	−1314.0	−1499.1	−409.5	594.6	−221.5			
Ce	Br	−1328.0	−1509.8	−440.8	622.6	−219.7			
Pr	Br	−1338.3	−1517.1	−478.5	657.3	−221.8			
Nd	Br	−1349.5	−1524.9	−529.3	704.7	−223.2			
Pm	Br	−1357.6	−1531.2	−540.2	713.8	−234.2			
Sm	Br	−1365.7	−1537.6	−549.6	721.4	−224.0			
Eu	Br	−1374.0	−1540.7	−561.2	727.9	−203.9			
Gd	Br	−1381.8	−1546.4	−574.5	739.1	−226.9			
Tb	Br	−1388.2	−1551.6	−584.4	747.8	−225.6			
Dy	Br	−1393.5	−1556.9	−591.3	754.7	−226.4			
Ho	Br	−1399.0	−1562.5	−600.0	763.5	−225.9			
Er	Br	−1403.0	−1568.1	−607.3	772.4	−223.3			
Tm	Br	−1407.0	−1574.0	−615.1	782.1	−220.5			
Yb	Br	−1411.0	−1580.2	−623.4	792.7	−204.8			
Lu	Br	−1415.0	−1586.5	−632.0	803.5	−220.2			
La	I	−1299.0	−1464.3	−552.7	718.0	−200.6			
Ce	I	−1312.8	−1472.3	−576.8	736.2	−198.5			
Pr	I	−1322.5	−1480.5	−593.4	751.4	−200.2			
Nd	I	−1332.8	−1488.6	−611.9	767.7	−200.5			
Pm	I	−1340.8	−1496.9	−627.3	783.4	−211.5			
Sm	I	−1348.5	−1504.6	−642.5	798.6	−200.9			
Eu	I	−1355.8	−1512.6	−657.9	814.6	−179.8			
Gd	I	−1361.7	−1520.4	−671.3	830.0	−200.8			
Tb	I	−1367.7	−1528.1	−685.2	845.6	−199.2			
Dy	I	−1373.7	−1535.8	−700.0	862.0	−200.6			
Ho	I	−1379.7	−1543.5	−714.9	878.7	−200.6			
Er	I	−1385.6	−1550.8	−729.8	895.0	−200.0			
Tm	I	−1390.9	−1588.0	−744.0	911.0	−198.4			
Yb	I	−1395.8	−1564.9	−757.0	926.0	−183.7			
Lu	I	−1399.8	−1571.8	−769.3	941.2	−199.1			

thought to be among the products of these wall reactions. Moreover, the triiodides are extremely hygroscopic and any absorbed water converts the volatile rare-earth iodides to HI plus involatile oxyiodides during the lamp processing. A quantitative understanding of these reactions requires thermodynamic descriptions of all pertinent species. Among the least known are the thermodynamic descriptions of the oxyiodide solids.

Table 1 gives the known thermodynamics data for the oxyhalides which have the tetragonal PbFCl structure P4/*nmm*. One sees in the last three columns that only the oxychlorides have measured enthalpies of formation. Some underlying theoretical framework is necessary if, from these measured oxychloride values, estimates are to be provided for the enthalpies of formation of the oxyiodides. Furthermore, this theoretical framework ought also to allow a description of the oxybromides as being in some sense intermediate.

Our previous work on the rare earth monohalide gaseous species [1], dihalide gaseous species [2], and trihalide solid and gaseous species [3] have shown that the framework needed is the enthalpy of formation of these species ⊖ not from their standard states but rather from their gaseous ions, i.e. the Rittner [4] energy. We call this enthalpy W_t. By means of Born–Haber cycles we obtain from W_t the desired $\Delta H^{\ominus}_{f,298}$, using well-known values for the enthalpies of vaporization of the metals and of the condensed-phase halogens, the ionization potentials, the electron affinities, and the dissociation energies of the halogen molecules. This approach is applied to the oxyhalide solid species in this paper.

In order to calculate W_t, we need interatomic distances. The interatomic distances used here come from crystallographic parameters. Table 2 gives, on those lines with references listed without the # sign, the relevant crystallographic structure parameters known from the literature, namely, a, c, u_M, and u_X. Only six of the oxyiodides have been measured. Moreover, as is discussed below, there are serious difficulties with the values reported for the oxybromides. Thus before we can start the estimates for the enthalpies, we need estimates for and some critical judgment about the crystallographic structure parameters. Our judgments and estimates are described in this paper.

TABLE 2

Crystallographic data for oxyhalide phases

M	X	a	c	u_m	u_x	Ref. [a]
La	Cl	4.119	6.883	0.178	0.635	6
		4.1209	6.8840			34–1494
		4.119	6.883	0.178	0.635	#1, #2
Ce	Cl	4.080	6.831			6
		4.080	6.831	0.1779	0.6361	#1, #2

TABLE 2 (continued)

M	X	a	c	u_m	u_x	Ref. [a]
Pr	Cl	4.051	6.810	0.18	0.64	6
		4.051	6.802			9-385
		4.051	6.810	0.1778	0.6372	#1, #2
Nd	Cl	4.018	6.782	0.18	0.64	6
		4.025	6.775			8–46
		4.018	6.782	0.1777	0.6383	#1, #2
Pm	Cl	4.023	6.773			33–1089
		4.002	6.747	0.1776	0.6383	#1, #2
Sm	Cl	3.982	6.721	0.17	0.63	6
		3.982	6.721	0.1775	0.6404	#1, #2
Eu	Cl	3.965	6.695			6
		3.9646	6.695	0.170	0.630	7
		3.965	6.695	0.1774	0.6415	#1, #2
Gd	Cl	3.950	6.672			6
		3.950	6.672	0.1772	0.6425	#1, #2
Tb	Cl	3.927	6.645			6
		3.927	6.645	0.1771	0.6436	#1, #2
Dy	Cl	3.911	6.620			6
		3.911	6.620	0.1770	0.6447	#1, #2
Ho	Cl	3.893	6.602	0.17	0.63	6
		3.893	6.602	0.1769	0.6457	#1, #2
Er	Cl	3.88	6.58			6
		3.873	6.580	0.1768	0.6468	#1, #2
Tm	Cl	3.850	6.560	0.1767	0.6479	#1, #2
Yb	Cl	3.850	6.560			31–1452
		3.830	6.542	0.1766	0.6489	#1, #2
Lu	Cl	3.810	6.526	0.1765	0.6500	#1, #2
La	Br	4.145	7.359	0.164	0.635	6
		4.159	7.392	0.1622	0.6349	9
		4.158	7.392			16–783
		4.144	7.361	0.1643	0.6340	#1
		4.132	7.472	0.1643	0.6500	#2
Ce	Br	4.130	7.494	0.1606	0.6391	#1
		4.098	7.564	0.1606	0.6520	#2
Pr	Br	4.08	7.49			16–782
		4.059	7.618	0.1572	0.6438	#1
		4.070	7.683	0.1572	0.6540	#2
Nd	Br	4.017	7.619	0.16	0.64	6
		4.0287	7.6302			37–1284
		4.021	7.731	0.1539	0.6482	#1
		4.041	7.791	0.1541	0.6560	#2
Pm	Br	3.986	7.834	0.1509	0.6521	#1
		4.020	7.970	0.1509	0.6580	#2
Sm	Br	3.95	7.91			16–784
		3.952	7.914			7
		3.945	7.904	0.1464	0.6550	9
		3.953	7.928	0.1480	0.6557	#1
		3.999	8.050	0.1480	0.6600	#2

TABLE 2 (continued)

M	X	a	c	u_m	u_x	Ref. [a]
Eu	Br	3.926	8.019			6
		3.924	8.015	0.145	0.660	7
		3.924	8.015			16–785
		3.923	8.011	0.1454	0.6589	#1
		3.980	8.130	0.1454	0.6612	#2
Gd	Br	3.91	8.15			16–786
		3.895	8.084	0.1430	0.6617	#1
		3.962	8.209	0.1430	0.6725	#2
Tb	Br	3.870	8.148	0.1408	0.6641	#1
		3.945	8.290	0.1408	0.6641	#2
Dy	Br	3.85	8.22			18–488
		3.848	8.201	0.1388	0.6661	#1
		3.928	8.366	0.1388	0.6661	#2
Ho	Br	3.828	8.244	0.1370	0.6677	#1
		3.911	8.429	0.1370	0.6677	#2
Er	Br	3.812	8.278	0.1354	0.6689	#1
		3.894	8.483	0.1354	0.6689	#2
Tm	Br	3.81	8.29			18–1376
		3.797	8.301	0.1341	0.6697	#1
		3.877	8.521	0.1341	0.6700	#2
Yb	Br	3.79	8.32			18–1465
		3.7847	8.309	0.133	0.670	7
		3.786	8.314	0.1329	0.6702	#1
		3.860	8.549	0.1329	0.6710	#2
Lu	Br	3.77	8.35			20–653
		3.777	8.317	0.1320	0.6702	#1
		3.843	8.567	0.1320	0.6720	#2
La	I	4.144	9.126	0.135	0.66	7
		4.144	9.126	0.1350	0.6600	#1, #2
Ce	I	4.116	9.149	0.1342	0.6619	#1, #2
Pr	I	4.086	9.162			34–829
		4.089	9.169	0.1334	0.6642	#1, #2
Nd	I	4.042	9.2484			37–1285
		4.064	9.185	0.1326	0.6664	#1, #2
Pm	I	4.01	9.18			34–543
		4.039	9.198	0.1318	0.6684	#1, #2
Sm	I	4.016	9.21			6
		4.008	9.192			16–48
		4.017	9.208	0.1310	0.6703	#1, #2
Eu	I	3.995	9.215	0.1302	0.6721	#1, #2
Gd	I	3.975	9.219	0.1293	0.6737	#1, #2
Tb	I	3.94	9.16			18–1333
		3.956	9.219	0.1285	0.6753	#1, #2
Dy	I	3.936	9.181			36–753
		3.938	9.217	0.1276	0.6767	#1, #2
Ho	I	3.921	9.211	0.1267	0.6780	#1, #2
Er	I	3.906	9.202	0.1258	0.6792	#1, #2
Tm	I	3.895	9.184	0.125	0.68	6

TABLE 2 (continued)

M	X	a	c	u_m	u_x	Ref. [a]
		3.887	9.166			15–650
		3.892	9.190	0.1249	0.6802	#1, #2
Yb	I	3.878	9.179			6
		3.870	9.161			16–60
		3.880	9.174	0.1240	0.6811	#1, #2
Lu	I	3.868	9.156	0.1231	0.6819	#1, #2

[a] The hyphenated entries are the identification numbers from the JCPDS–ICDD database [8]; for the meaning of #1 and #2, see text.

Crystal structure

In the tetragonal PbFCl structure (#129, ref. 5), the unit cell contains two formula units. The metals occupy ($2c$) positions at (0,0.5,u_m) and at (0.5,0,$-u_m$), the halogens are in ($2c$) positions at (0,0.5,u_x) and (0.5,0,$-u_x$), and the oxygens are in ($2a$) positions at (0,0,0) and (0.5,0.5,0) [6].

Each metal ion is surrounded by eight or nine anions: four oxygen anions on one side in a square planar configuration and four halogen anions on the other side, also in a square planar configuration but rotated by 45° relative to the oxygen square.

The structure has blocks of X–M–O–M–X layers in sequence along the c axis. Each block is held together by very strong M–O bonds, strong enough to produce smaller than expected M–O distances and to put the larger halide ions into compression. In the oxychlorides the X ions of each block are near M ions of neighboring blocks, introducing a ninth anion into the coordination sphere of the metal. This extra M–X bond formed thereby holds the blocks together to generate a three-dimensional network. In the oxyiodides, this inter-layer M–X bonding is much weaker than in the oxychlorides. The blocks are bonded to each other by van der Waals forces only and the result is a layered structure. In the oxybromides, a transitional situation is found: the oxybromides of the heavier and therefore smaller rare-earths resemble the oxyiodides, because the ratio of halide size to metal size is large; those of the lighter and therefore larger rare-earths resemble the oxychlorides because the ratio of halide size to metal size is small. This structure was described by Bärnighausen et al. (BBS) [7].

As described above, the literature values for the lattice dimensions and positional coordinates are given in Table 2. The crystal structures were taken from Wyckoff [6], from the JCPDS–ICDD 1991 database [8] (which gives their original references), from BBS [7], and from Häuseler and Jung [9].

Also shown in Table 2 and identified with the label "#1" in the reference column are values obtained by fitting the literature data to smooth curves.

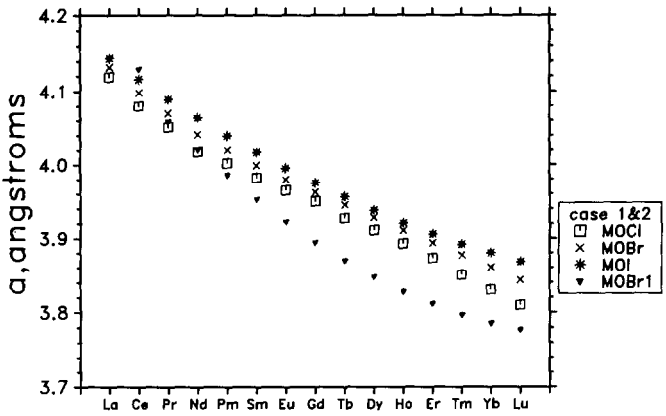

Fig. 1. The *a* lattice parameters. The values adopted here for all halides are indicated by the label #2; also plotted (as filled triangles) are values from the literature and values interpolated therefrom for the oxybromides; these are denoted by the label #1 (Table 2).

The values labeled "#2" are those adopted here because they show smoother trends in bond distances and in calculated energies. The justification for choice #2 is described below.

The *a* parameters, *c* parameters, *c*/*a* ratios, u_x values, and u_m values are plotted in Figs. 1–5, respectively. In Figs. 1–5, the values plotted for all halides are those identified as "#2" in Table 2. In addition, the set identified as "#1" in Table 2 is also plotted for the oxybromides and labeled "MOBr1".

There is something wrong with the #1 oxybromide values. Every expectation is that the oxybromide *a* values would be intermediate between the oxychloride and the oxyiodide values. The #1 oxybromide values clearly violate this expectation. They lie below the values for both the

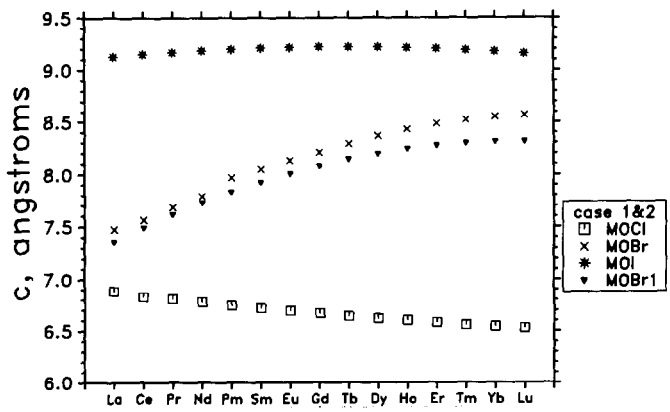

Fig. 2. The *c* lattice parameters. The values adopted here for all halides are indicated by the label #2; also plotted (as filled triangles) are literature values for the oxybromides denoted by the label #1 (Table 2).

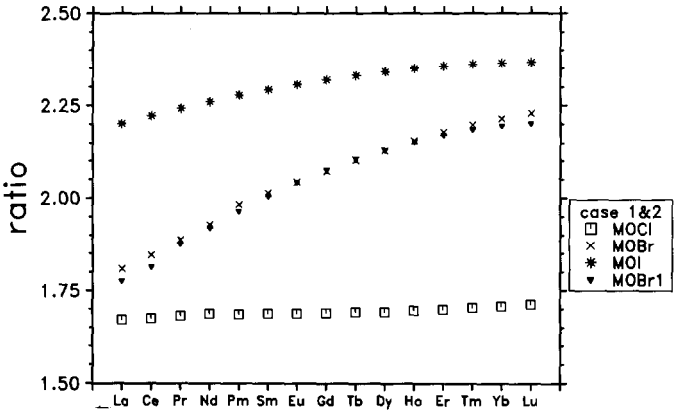

Fig. 3. The c/a ratios. The ratios shown using our adopted values for c and a for all halides are indicated by the label #2; also plotted are ratios of the literature-derived values for c and a for the oxybromides; these are referenced by the label #1 (Table 2).

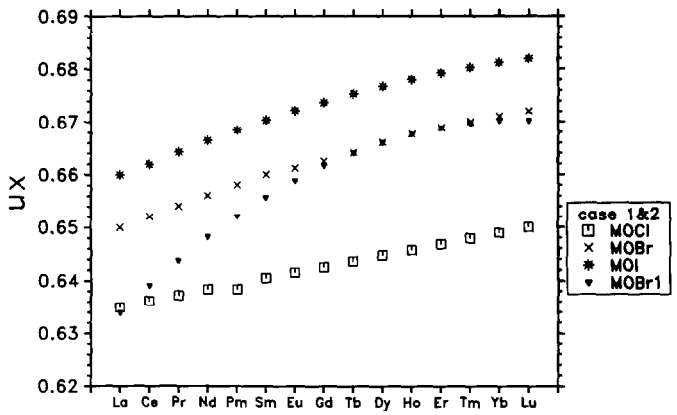

Fig. 4. The u_x values. The values shown are those adopted here for all halides and are indicated by the label #2; also plotted (as filled triangles) are values derived from the literature for the oxybromides; these are referenced by the label #1 (Table 2).

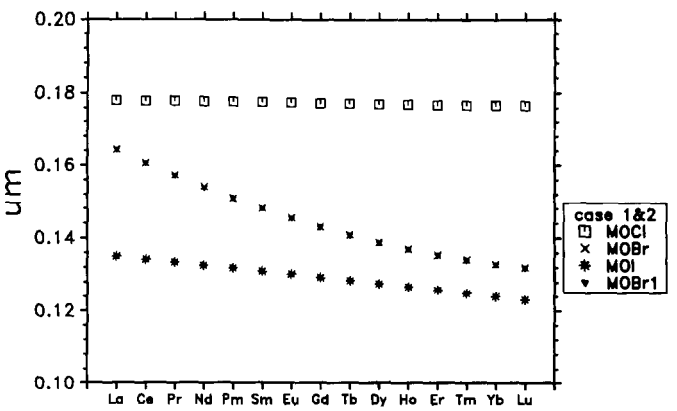

Fig. 5. The u_m values. The values shown are those adopted here for all halides and are indicated by the label #2; also plotted (as filled triangles) are values derived from the literature for the oxybromides; these are referenced by the label #1 (Table 2).

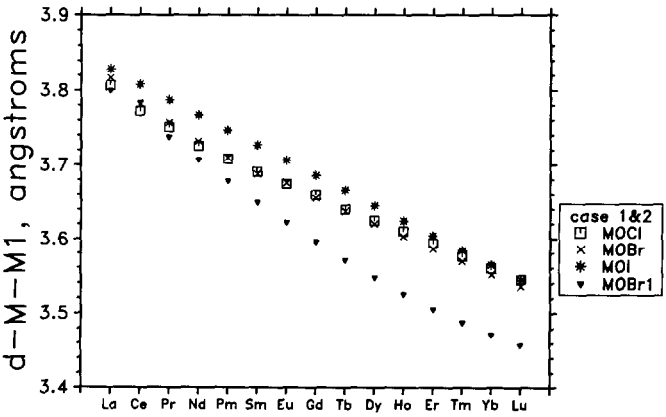

Fig. 6. The nearest neighbor M–M distances. The values shown are those adopted here for all halides and are indicated by the label #2; also plotted (as filled triangles) are values calculated from the literature descriptions of the oxybromides; these are referenced by the label #1.

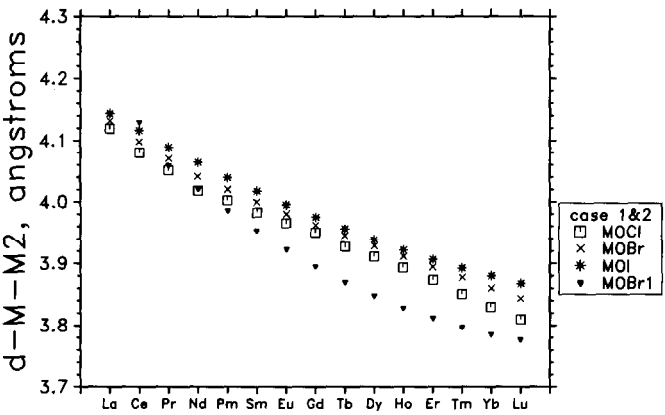

Fig. 7. The second-nearest neighbor M–M distances. The values shown are those adopted here for all halides and are indicated by the label #2; also plotted (as filled triangles) are values calculated from the literature descriptions of the oxybromides; these are referenced by the label #1.

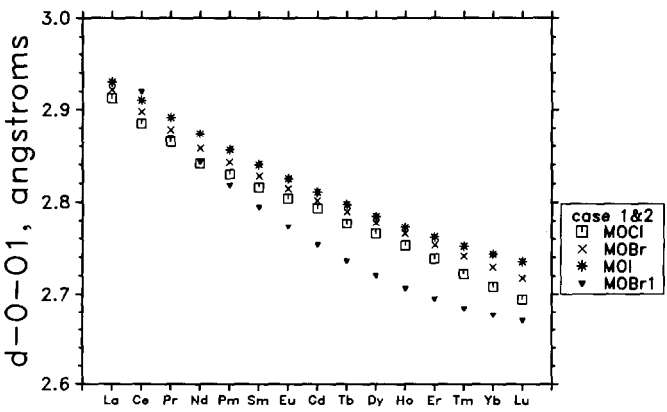

Fig. 8. The nearest neighbor O–O distances. The values shown are those adopted here for all halides and are indicated by the label #2; also plotted (as filled triangles) are values calculated from the literature descriptions of the oxybromides; these are referenced by the label #1.

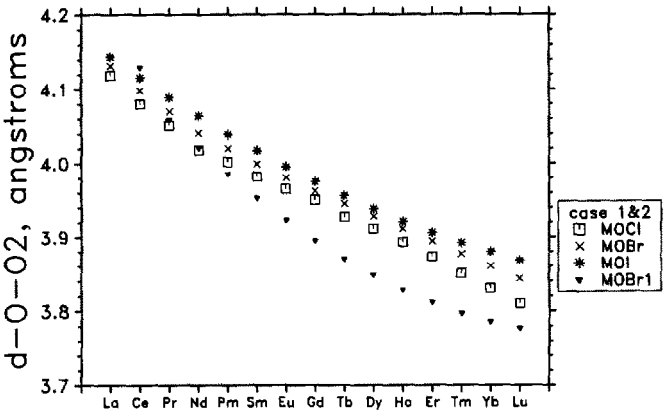

Fig. 9. The second-nearest neighbor O–O distances. The values shown are those adopted here for all halides and are indicated by the label #2; also plotted (as filled triangles) are values calculated from the literature descriptions of the oxybromides; these are referenced by the label #1.

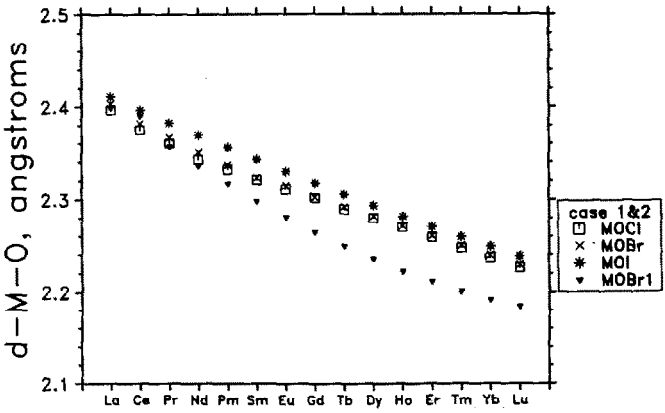

Fig. 10. The nearest neighbor M–O distances. The values shown are those adopted here for all halides and are indicated by the label #2; also plotted (as filled triangles) are values calculated from the literature descriptions of the oxybromides; these are referenced by the label #1.

oxychlorides and the oxyiodides. The same anomaly for case #1 is also evident in the nearest neighbor M–M distance, the second M–M distance, the nearest O–O distance, the second O–O distance, and the nearest M–O distance shown in Figs. 6–10.

Thermodynamic parameters

In their Table VI, Hisham and Benson [10] give experimental values for the standard enthalpy of formation of all rare earth oxychlorides except Pm. Weigel and Wishnevsky [11] give the standard enthalpy of formation of

TbOCl. Patrikeev et al. [12] give the standard enthalpy of formation of LaOCl. All these values are included in Table 1, with the appropriate references, along with the modeling results of this paper. Our estimates for the enthalpies of formation $\Delta H^{\ominus}_{f,298}$ are listed in Table 1 under the column headed "This work" and those from the literature are in the column labeled "Lit.". There are no experimental values known to us for the oxybromides or for the oxyiodides.

Modeling in the literature

In their eqn. (4), Hisham and Benson [10] estimated the enthalpy of formation of rare-earth oxychlorides, among other phases, by postulating the relationship

$$\Delta H^{\ominus}_{f,298}(MOCl) = a'[\tfrac{1}{3}\,\Delta H^{\ominus}_{f,298}(M_2O_3) + \tfrac{1}{3}\,\Delta H^{\ominus}_{f,298}(MCl_3)] + b' \quad (1)$$

These authors give $a' = 2.155 \pm 0.12$ and $b' = 257.8 \pm 1.3$ or $b' = 250.4 \pm 1.2$ kcal mol^{-1} as bracketing the observed values of the $\Delta H^{\ominus}_{f,298}(MOCl)$. We have no expectation that this line of reasoning will afford a general understanding of all oxyhalide thermodynamics, particularly because there is no way to obtain the fitting parameters a' and b' for oxybromides and oxyiodides in the absence of experimental data.

There seems to be no underlying theory supporting such a correlation. If a' were unity, then the underlying concept would be that the enthalpy of dissociating the oxyhalide into oxide and halide

$$MOX \rightarrow \tfrac{1}{3}[MX_3 + M_2O_3]$$

is a constant across the rare-earth series. There is no reason to expect such a constancy for this dissociation enthalpy. However, we do expect that this dissociation enthalpy should show smooth behavior within the rare earth series and among the halides. This expectation arises because the $\Delta H^{\ominus}_{f,298}$ of this reaction and the ΔW_t of this reaction are identical. Born–Haber cycles relating these thermodynamic functions show all other terms canceling. Because the W_t values for the three phases across the rare-earth series are all smoothly varying, the enthalpy of the reaction must also be smoothly varying.

The enthalpy of formation of rare-earth oxides

To obtain values for dissociation enthalpies, one needs the enthalpies of formation of the oxide (listed in Table 3) and of the solid trihalide phases. The required standard enthalpies of the halides were taken from our paper [3].

The standard enthalpies of the oxides in the first column of Table 3 were taken from Pankratz [13]. The W_t values calculated from them are shown in

TABLE 3

$\Delta H^{\ominus}_{f,298}$ and W_t for rare-earth oxides

M	$\Delta H^{\ominus}_{f,298}$ [13]	W_t [13]	W_t (ours)	$\Delta H^{\ominus}_{f,298}$ (ours)
La	−428.7	−2930.2	−2930.2	−428.7
Ce	−429.3	−2962.4	−2961.8	−428.7
Pr	−432.5	−2981.8	−2981.8	−432.5
Nd	−432.1	−3001.3	−3002.1	−432.9
Pm			−3018.3	−455.0
Sm	−436.7	−3036.6	−3035.0	−435.1
Eu	−397.4	−3054.1	−3052.1	−395.4
Gd	−436.6	−3062.9	−3067.9	−441.6
Tb	−445.8	−3087.5	−3082.5	−440.8
Dy	−445.3	−3096.0	−3098.0	−447.3
Ho	−449.6	−3112.4	−3113.4	−450.6
Er	−453.6	−3129.5	−3128.5	−452.6
Tm	−451.4	−3141.0	−3141.0	−451.4
Yb	−433.7	−3162.6	−3152.6	−423.7
Lu	−448.9	−3155.0	−3162.0	−455.9

the second column. There is some irregular behavior in these W_t values, of the order of a few kcal mol^{-1} (but as large as 10 kcal mol^{-1} for Yb). Because the expected behavior is smooth, we imposed smoothness and obtained the values shown in the fourth column labeled "ours". The standard enthalpies of formation in the fifth column, again labeled "ours", were calculated from these smoothed W_t values.

Basis for a strategy invoking smoothness

We have previously published estimates of the enthalpy of formation of gaseous rare-earth monohalides [1], gaseous rare-earth dihalides [2], and both gaseous and solid rare-earth trihalides [3]. In each case our approach was to estimate the energy required to dissociate the pertinent species into gaseous ions ($-W_t$) and to obtain the desired enthalpies of formation $\Delta H^{\ominus}_{f,298}$ through use of a Born–Haber cycle. The W_t values vary smoothly with atomic number across the rare-earth series, whereas the $\Delta H^{\ominus}_{f,298}$ made 50 kcal mol^{-1} excursions from one rare-earth to the next in a series traceable to the jagged behavior of the ionization energies and the enthalpies of vaporization of these metals.

For the monohalides, we used the Rittner energy [4] expression to estimate these W_t values. The Rittner energy is the energy of a collection of polarizable charged particles. Our contribution was to create a set of polarizabilities which allowed fitting certain known values and interpolating extrapolating to obtain values for those that had not been measured.

For the dihalides, we used an extended Rittner energy expression,

extended by explicitly including a covalent energy contribution. We again created a set of energy parameters which allowed assessment of unknown enthalpies from the few which were known. Here, as in this work, there were more parameters to be determined than explicit data available to fix their values, and we relied on criteria of smoothness in the behavior of both parameters and calculated energies.

For the trihalides, there were enough known values to allow smoothing of the W_t values by least squares fitting for the chlorides, and we could create fitting parameters for the other halides which showed smooth halide-to-halide variation.

Approach used here

In the literature, the experimental values of $\Delta H^{\ominus}_{f,298}$ are known only for the oxychlorides and are listed in Table 1. From them, through a Born–Haber cycle, we determined W_t. As with the oxides discussed above, the W_t values are expected to vary smoothly across the rare earth series and from halide to halide. The W_t values derived from the $\Delta H^{\ominus}_{f,298}$ in the literature (listed in the ninth column of Table 1 and labeled as such) are not smooth (see especially the values for YbOCl and LuOCl in this column). By fitting these W_t values to a smooth curve, we obtained the set of W_t and the corresponding $\Delta H^{\ominus}_{f,298}$ for the oxychlorides shown in the third and seventh columns, respectively, of Table 1. The smoothed W_t values are plotted in Fig. 11.

We then computed from the $\Delta H^{\ominus}_{f,298}$ values for the oxychlorides the enthalpy of dissociation of the oxychlorides into oxide and chloride phases. These are shown in Fig. 12.

We then placed the oxyiodides so as to make their W_t values less stable than the oxychlorides, while maintaining a slight stability with respect to decomposition to the oxide and triiodide phases. After a few iterations, the

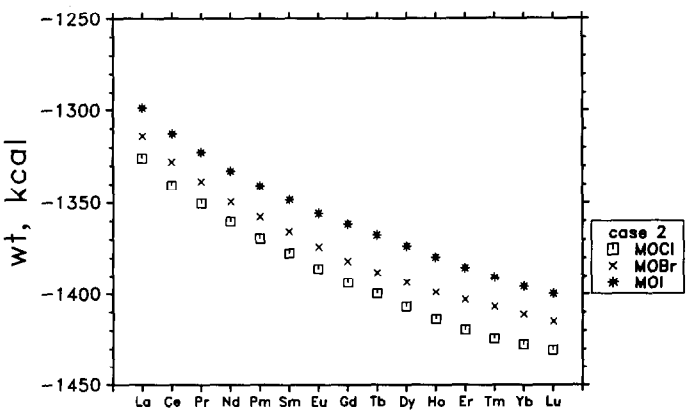

Fig. 11. The W_t values calculated here using the lattice parameters labeled #2 in Table 1 and the energy parameters listed in Table 4.

TABLE 4

Potential function parameters

M	X	D_O	A_O	B_O	D_X	A_X	B_X	D_M	A_M	B_M
La	Cl	158.53	2.3414	0.24839	125.35	2.6586	0.31061	6.2233	1.8550	0.10004
Ce	Cl	157.04	2.3391	0.24724	128.36	2.6386	0.30062	8.8812	1.8491	0.09951
Pr	Cl	156.57	2.3380	0.24666	136.43	2.6404	0.28224	12.451	1.8482	0.09734
Nd	Cl	156.81	2.3358	0.24514	139.14	2.5458	0.28109	13.505	1.8449	0.09845
Pm	Cl	155.77	2.3350	0.24444	139.61	2.6334	0.27685	15.684	1.8421	0.09800
Sm	Cl	156.73	2.3338	0.24447	142.34	2.6335	0.27473	16.146	1.8413	0.09775
Eu	Cl	156.97	2.3327	0.24413	143.83	2.6272	0.27153	17.377	1.8400	0.09734
Gd	Cl	157.11	2.3316	0.24388	145.07	2.6216	0.26875	18.436	1.8382	0.09698
Tb	Cl	158.95	2.3309	0.24422	141.82	2.6213	0.27044	18.936	1.8377	0.09705
Dy	Cl	159.08	2.3288	0.24398	142.53	2.6143	0.26779	19.206	1.8361	0.09703
Ho	Cl	158.84	2.3307	0.24309	135.66	2.5785	0.26734	20.938	1.8332	0.09712
Er	Cl	158.78	2.3301	0.24318	136.18	2.5765	0.26644	21.242	1.8323	0.09726
Tm	Cl	158.54	2.3296	0.24345	136.43	2.5767	0.26652	21.255	1.8316	0.09755
Yb	Cl	158.12	2.3292	0.24383	136.29	2.5780	0.26727	21.029	1.8310	0.09794
Lu	Cl	157.80	2.3289	0.24421	136.16	2.5795	0.26802	20.753	1.8306	0.09833
La	Br	185.23	2.4239	0.27617	179.09	2.8208	0.30490	22.163	2.0110	0.09890
Ce	Br	188.55	2.4166	0.27437	192.65	2.8542	0.30084	20.940	1.9970	0.09885
Pr	Br	188.17	2.4204	0.26943	202.60	2.8984	0.30240	24.455	1.9736	0.09940
Nd	Br	187.83	2.4246	0.26452	213.97	2.9426	0.30463	29.257	1.9587	0.10054
Pm	Br	186.87	2.4202	0.26306	221.17	2.9536	0.30153	28.967	1.9459	0.10053
Sm	Br	185.14	2.4165	0.26153	226.44	2.9570	0.29798	29.125	1.9334	0.10058
Eu	Br	184.44	2.4134	0.25998	233.09	2.9582	0.29320	29.737	1.9236	0.10026
Gd	Br	183.08	2.4107	0.25905	238.91	2.9611	0.29000	30.220	1.9157	0.10021
Tb	Br	181.43	2.4081	0.25809	243.27	2.9637	0.28778	30.742	1.9079	0.10015
Dy	Br	179.37	2.4057	0.25700	245.75	2.9652	0.28639	31.249	1.8991	1.10017
Ho	Br	177.39	2.4034	0.25604	248.12	2.9663	0.28507	31.863	1.8914	0.10014
Er	Br	175.39	2.4018	0.25562	249.95	2.9677	0.28431	32.306	1.8863	0.10027
Tm	Br	173.39	2.4001	0.25508	250.80	2.9680	0.28384	32.804	1.8807	0.10038
Yb	Br	171.34	2.3986	0.25458	251.28	2.9678	0.28351	33.324	1.8754	0.10049
Lu	Br	169.39	2.3970	0.25387	250.77	2.9667	0.28346	33.908	1.8691	0.10052
La	I	204.66	2.4734	0.27905	318.51	3.2647	0.33494	32.297	2.0237	0.09907
Ce	I	202.64	2.4702	0.27582	317.43	3.2433	0.32877	34.918	2.0085	0.09826
Pr	I	199.82	2.4681	0.27346	314.02	3.2274	0.32565	36.931	1.9957	0.09796
Nd	I	197.19	2.4657	0.27101	310.66	3.2218	0.32245	39.200	1.9829	0.09750
Pm	I	194.22	2.4637	0.26917	306.88	3.2000	0.32074	41.065	1.9720	0.09729
Sm	I	191.50	2.4617	0.26747	303.26	3.1892	0.31918	42.945	1.9621	0.09701
Eu	I	188.71	2.4596	0.26593	299.54	3.1794	0.31801	44.794	1.9527	0.09675
Gd	I	185.92	2.4579	0.26487	296.56	3.1725	0.31742	46.287	1.9452	0.09666
Tb	I	183.29	2.4561	0.26372	293.27	3.1656	0.31692	47.846	1.9375	0.09650
Dy	I	180.70	2.4542	0.26272	290.78	3.1597	0.31632	49.368	1.9305	0.09635
Ho	I	178.15	2.4522	0.26178	288.41	3.1539	0.31569	50.882	1.9238	0.09618
Er	I	175.74	2.4503	0.26088	286.47	3.1489	0.31505	52.377	1.9174	0.09599
Tm	I	173.40	2.4485	0.26017	285.00	3.1450	0.31452	53.676	1.9118	0.09588
Yb	I	171.15	2.4468	0.25956	283.82	3.1417	0.31403	54.856	1.9066	0.09579
Lu	I	168.84	2.4455	0.25914	282.98	3.1399	0.31392	55.843	1.9021	0.09584

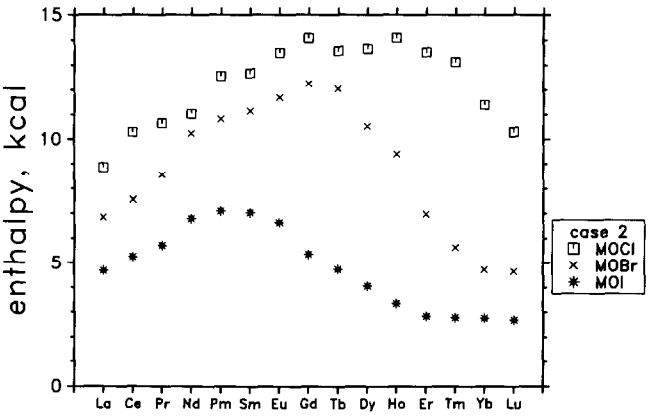

Fig. 12. The enthalpy to dissociate oxyhalides into oxide and halide solid phases. The standard enthalpy of formation of the oxyhalides and of the oxides are those marked "ours" in Tables 1 and 3, respectively. The standard enthalpies of formation of the halides were taken from ref. 3.

values of W_t for the oxyiodides in Fig. 11 and the corresponding energies of dissociation in Fig. 12 resulted.

The oxybromides were placed at intermediate energy values, with some effort to allow a transition from chloride-like to iodide-like behavior with increasing atomic number.

In this way, we have created the complete set of W_t values shown in Table 1 and Fig. 11. Also included are the $\Delta H^{\ominus}_{f,298}$ values calculated from these W_t values using the same Born–Haber cycle. The parameters needed for these Born–Haber cycles are from ref. 2, Tables 1, 2 and 6, with the electron affinity of O^{2-} as +155 kcal mol^{-1}.

The use of lattice sums

We have attempted to give credibility to these adopted W_t values through the use of two-bodied potential functions summed over the infinite lattice. We use the lattice energy program of Busing [14], which uses his potential energy expression [15], namely

$$W_t = \tfrac{1}{2}\sum_i \sum_j \left[\frac{q_i q_j}{r_{ij}} - \frac{D_i D_j}{r_{ij}^6} + f(B_i + B_j) \exp \frac{A_i + A_j - r_{ij}}{B_i + B_j} \right] \quad (2)$$

where q_i is the full charge on the ith ion (e.g. +3 for the rare earths), D (in units of energy$^{1/2}$ × volume) is described as a coefficient related to the ionic polarizability, B is a hardness parameter with dimensions of length, and A is a radius of the ion. The first term is the coulombic energy, the second a "van der Waals" energy, and the third is a repulsive energy. In order for the repulsive energy to have the proper units, the f factor is introduced, set equal to unity, and given dimensions energy × length^{-1}.

Busing used this potential function to search for a unique set of D_i, A_i and B_i values for the ith ion in every species. Here, the number of such parameters would be 18×3, i.e. 3 for each of the 18 different atomic species. We have found that this approach led to no understanding at all of the enthalpies of formation across the three oxyhalide series.

In order to obtain a consistency between calculated crystal energies and our expected W_t values, we have had to search for values for each ion which are different in different lattices. A nonconstant value is indeed more plausible behavior, because the charge-induced-dipole energy and the other energy terms determined by polarization effects depend not only on the polarizability of an ion but also on the field at that ion position due to the presence of all other ions and induced dipoles. These fields are not expected to be identical for M^{3+} in all oxyhalides, nor are they expected to vary as the inverse sixth power of the separation distance.

There are now 9 parameters for each of the 45 LnOX species, 405 in all. To restore uniqueness, we need to postulate an alternative to the constraint of constancy invoked by Busing. We choose smoothness in the parameter values across the rare earth series and from halide to halide. We also invoke the same smoothness in all the energies calculated using these parameters.

RESULTS

Table 4 and Figs. 13–21 show the set of parameters adopted here. These energy parameters, together with the crystallographic parameters labeled #2 in Table 2, are the set of parameters which yields maximum smoothness in the fit. These parameters yield the W_t and the related $\Delta H^{\ominus}_{f,298}$ values listed in Table 1. The W_t values are sums of the crystal energy W_c, the van der Waals energy W_v, and the repulsive energy W_r, which are also listed in Table 1. These energies are shown plotted in Figs. 11 and 22–24, respectively.

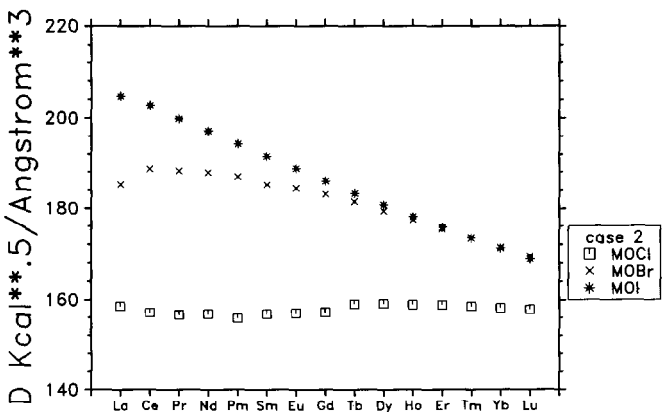

Fig. 13. The D_O parameters adopted here. These are the van der Waals energy parameters in eqn. (2) for the divalent oxygen ion. They are seen to vary from rare earth to rare earth and from halogen to halogen in LnOX.

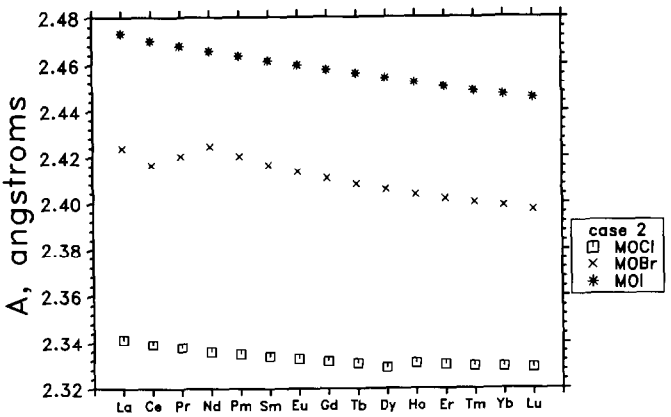

Fig. 14. The A_O parameters adopted here. These are parameters in eqn. (2) for the divalent oxygen ion in the repulsive energy term.

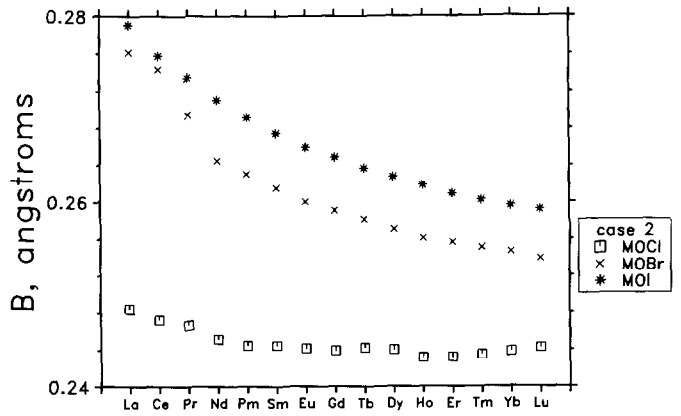

Fig. 15. The B_O parameters adopted here. These are parameters in eqn. (2) for the divalent oxygen ion in the repulsive energy term.

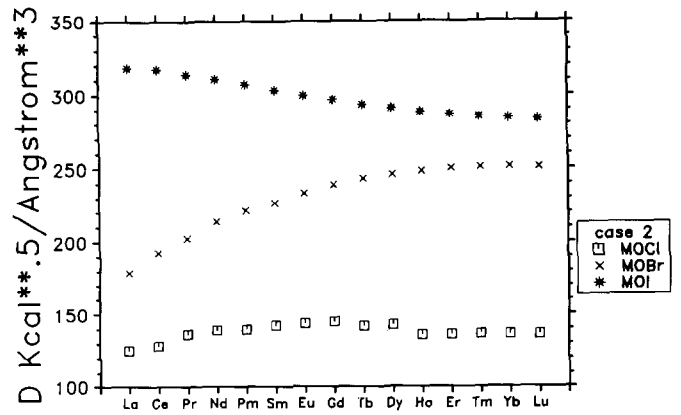

Fig. 16. The D_X parameters adopted here. These are parameters in eqn. (2) for the halide ion in the van der Waals energy term.

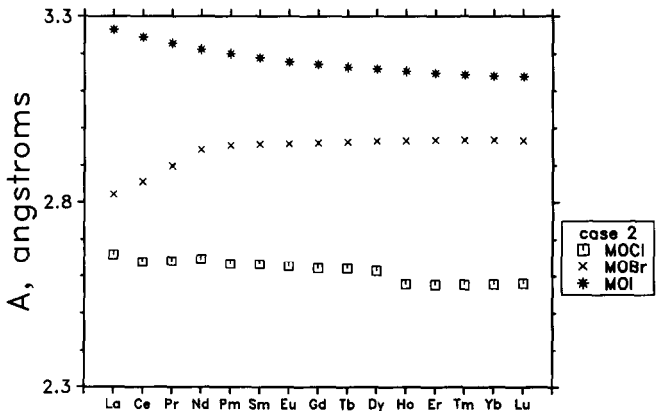

Fig. 17. The A_X parameters adopted here. These are parameters in eqn. (2) for the halide ion in the repulsive energy term.

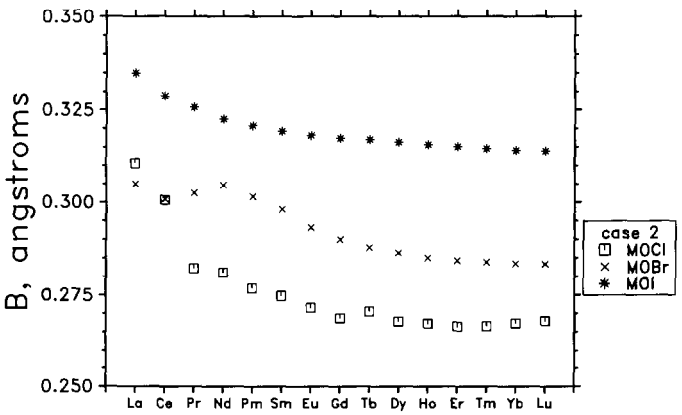

Fig. 18. The B_X parameters adopted here. These are parameters in eqn. (2) for the halide ion in the repulsive energy term.

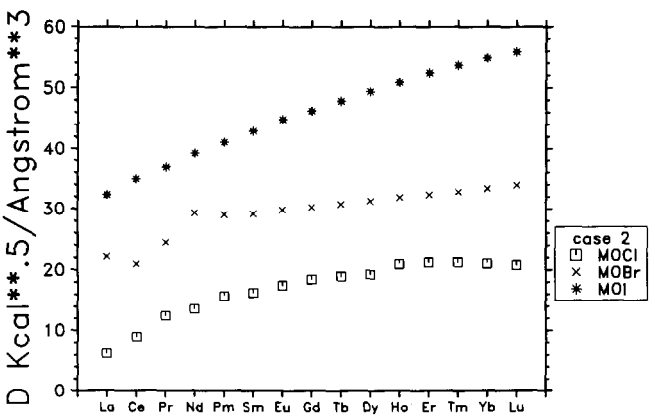

Fig. 19. The D_M parameters adopted here. These are parameters in eqn. (2) for the metal ion in the van der Waals energy term.

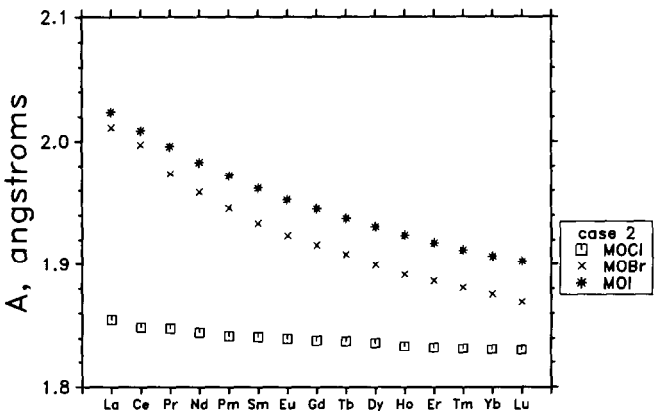

Fig. 20. The A_M parameters adopted here. These are parameters in eqn. (2) for the metal ion in the repulsive energy term.

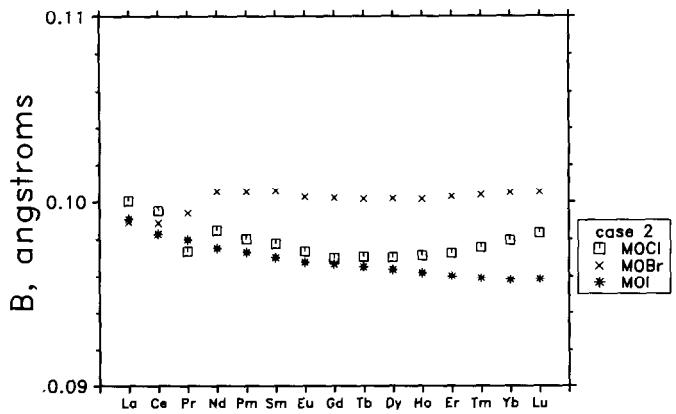

Fig. 21. The B_M parameters adopted here. These are parameters in eqn. (2) for the metal ion in the repulsive energy term.

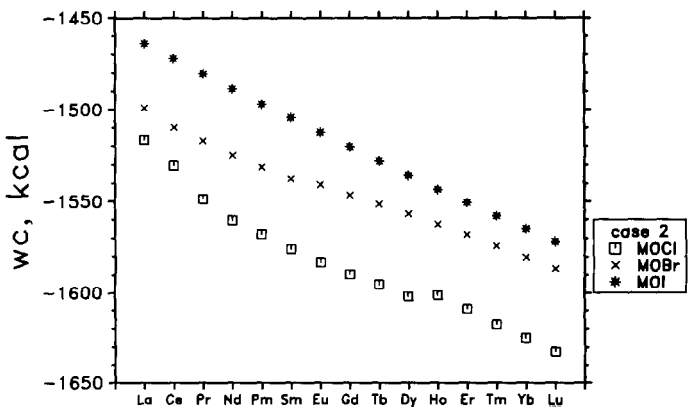

Fig. 22. The coulombic energy W_c calculated here, using the lattice parameters labeled #2 in Table 2. This energy is summed over all lattice sites.

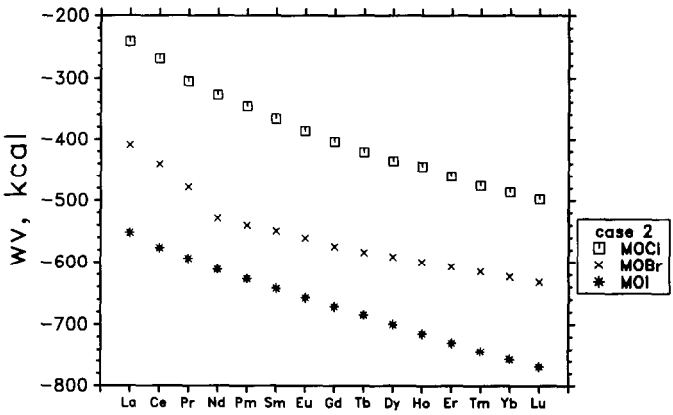

Fig. 23. The total van der Waals energy W_v calculated here, using the lattice parameters labeled #2 in Table 2 and the D parameters listed in Table 4.

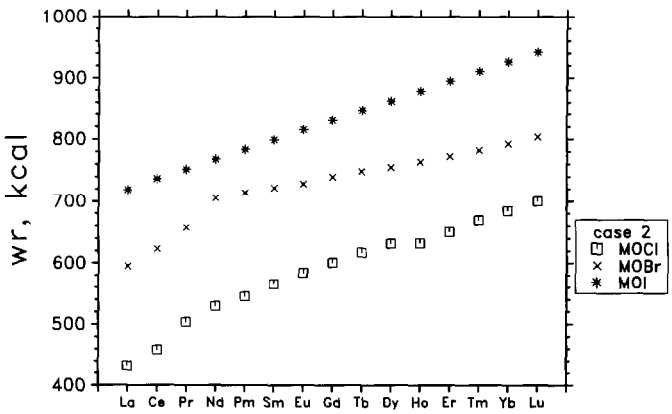

Fig. 24. The total repulsive energy W_r calculated here, using the lattice parameters labeled #2 in Table 2, and the A and B parameters listed in Table 4.

The individual coulombic, van der Waals, and repulsive energies for the nearest neighbor M–M bond have the smooth dependences shown in Figs. 25–27, respectively. This group of three quantities is also given for ten other near-neighbor bonds in Figs. 28–57.

The total van der Waals energy is a factor of 100 larger than expected and is to be interpreted as containing polarization effects and also covalent effects. The total repulsive energy is somewhat greater than we expected. The balancing "van der Waals" and repulsive energies are both made compensatingly high by the Busing program in order to obtain the slope of all the energy vs. lattice-parameter curves equal to zero at the chosen lattice dimensions, u parameters, and W_t values.

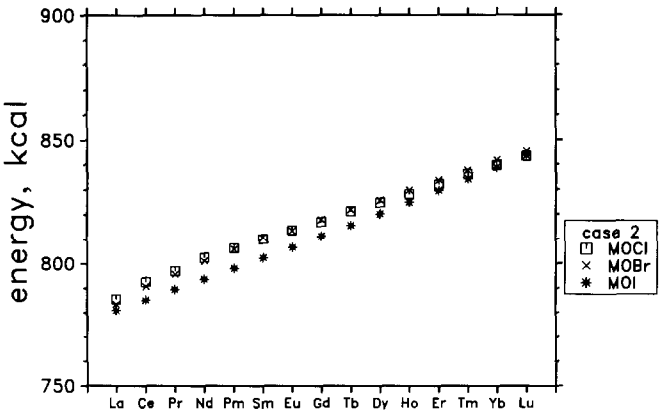

Fig. 25. The coulombic energy of the nearest neighbor M–M bonds, as calculated here using the lattice parameters labeled #2 in Table 2.

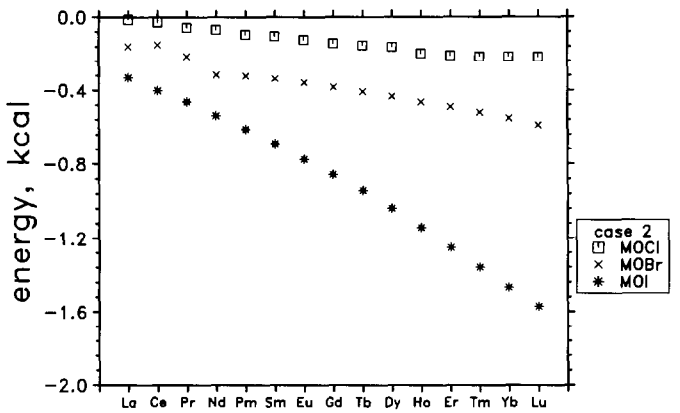

Fig. 26. The van der Waals energy of the nearest neighbor M–M bond, as calculated here using the lattice parameters labeled #2 in Table 2 and the *D* energy parameters listed in Table 4.

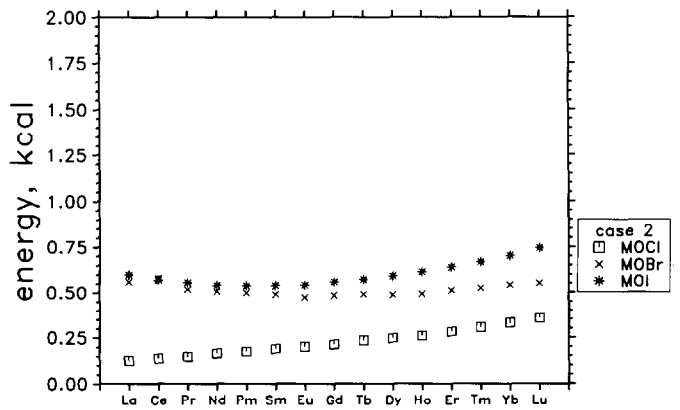

Fig. 27. The repulsive energy of the nearest neighbor M–M bond, as calculated here using the lattice parameters labeled #2 in Table 2 and the *A* and *B* energy parameters listed in Table 4.

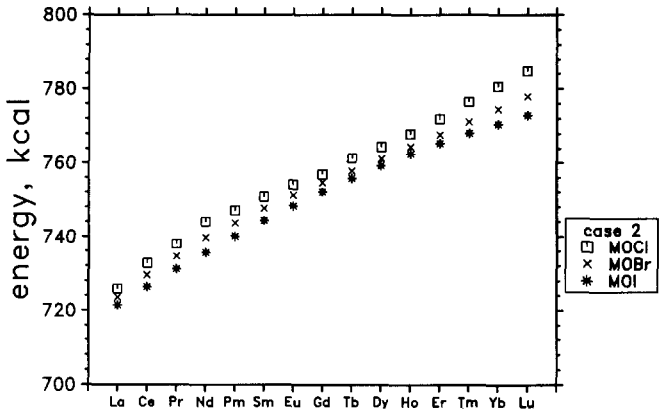

Fig. 28. The coulombic energy of the second-nearest neighbor M–M bond, as calculated here using the lattice parameters labeled #2 in Table 2.

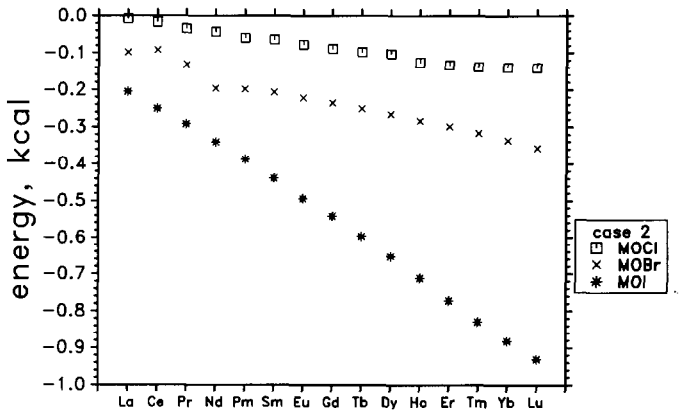

Fig. 29. The van der Waals energy of the second-nearest neighbor M–M bond, as calculated here using the lattice parameters labeled #2 in Table 2 and the D energy parameters listed in Table 4.

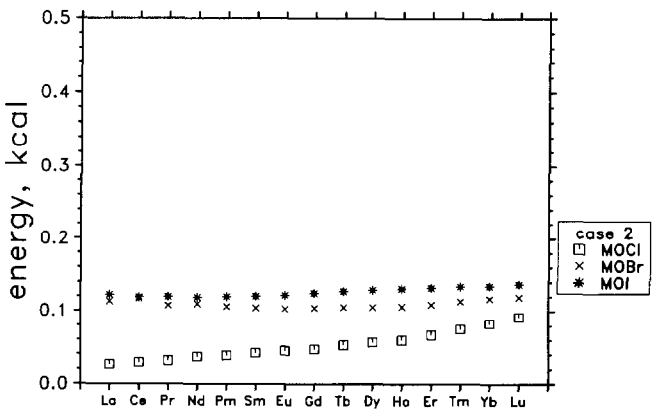

Fig. 30. The repulsive energy of the second-nearest neighbor M–M bond, as calculated here using the lattice parameters labeled #2 in Table 2 and the A and B energy parameters listed in Table 4.

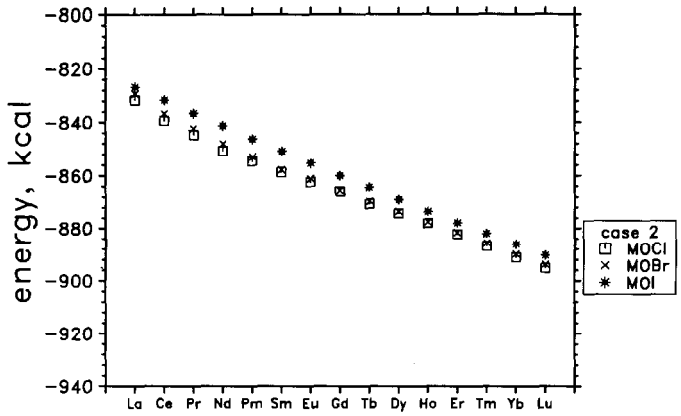

Fig. 31. The coulombic energy of the nearest neighbor M–O bond, as calculated here using the lattice parameters labeled #2 in Table 2.

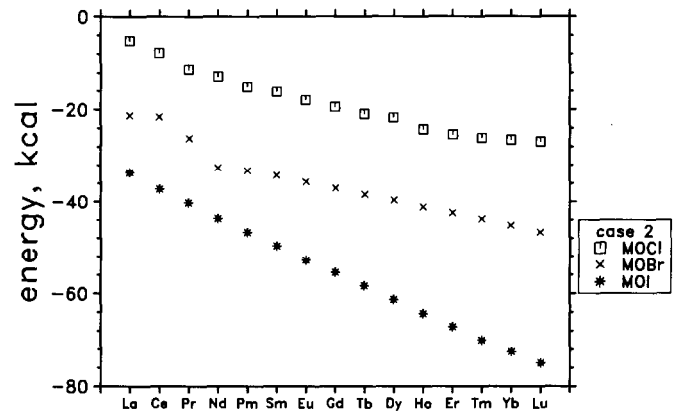

Fig. 32. The van der Waals energy of the nearest neighbor M–O bond, as calculated here using the lattice parameters labeled #2 in Table 2 and the *D* energy parameters listed in Table 4.

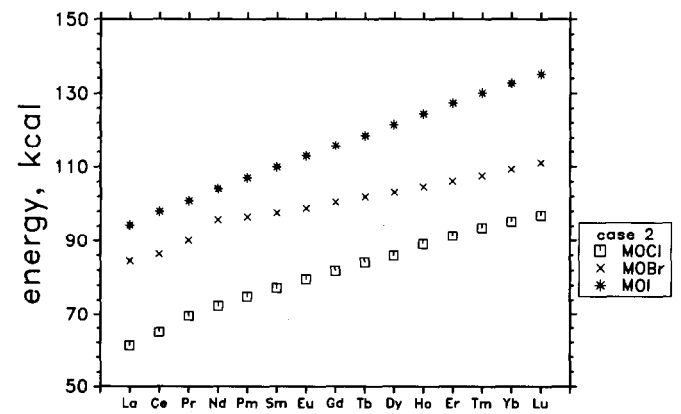

Fig. 33. The repulsive energy of the nearest neighbor M–O bond, as calculated here using the lattice parameters labeled #2 in Table 2 and the *A* and *B* energy parameters listed in Table 4.

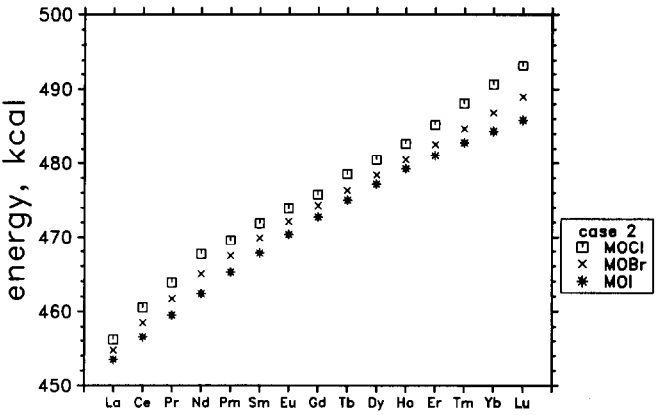

Fig. 34. The coulombic energy of the nearest neighbor O–O bond, as calculated here using the lattice parameters labeled #2 in Table 2.

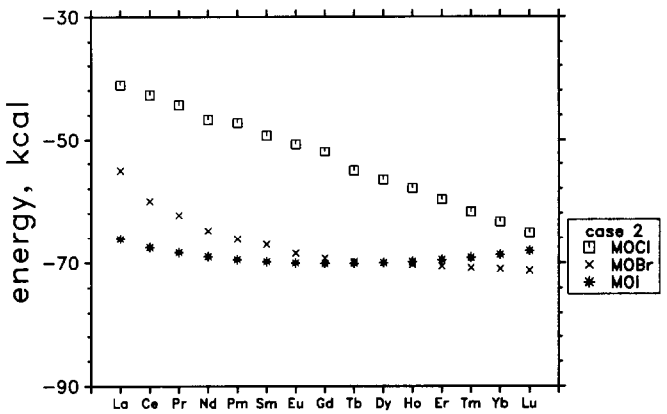

Fig. 35. The van der Waals energy of the nearest neighbor O–O bond, as calculated here using the lattice parameters labeled #2 in Table 2 and the *D* energy parameters listed in Table 4.

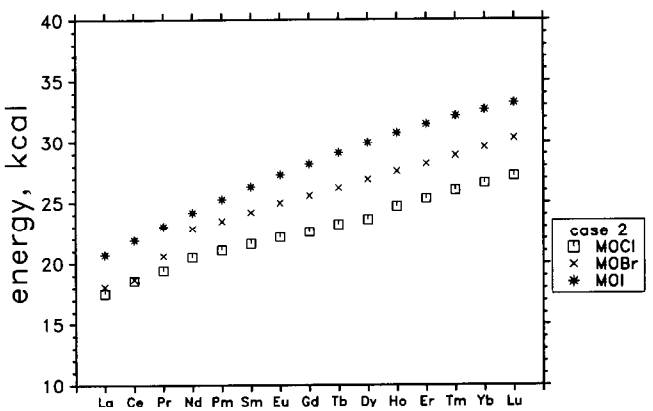

Fig. 36. The repulsive energy of the nearest neighbor O–O bond, as calculated here using the lattice parameters labeled #2 in Table 2 and the *A* and *B* energy parameters listed in Table 4.

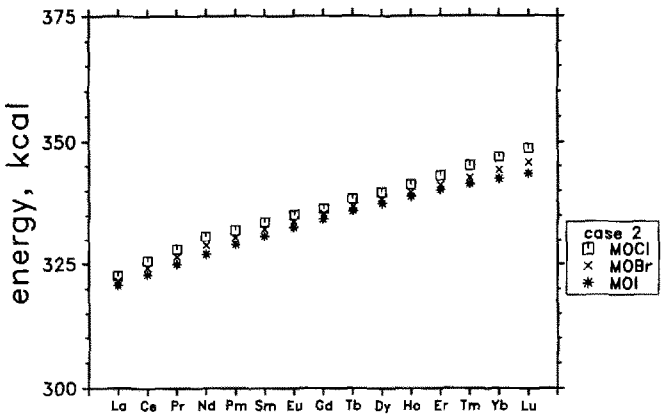

Fig. 37. The coulombic energy of the second-nearest neighbor O–O bond, as calculated here using the lattice parameters labeled #2 in Table 2.

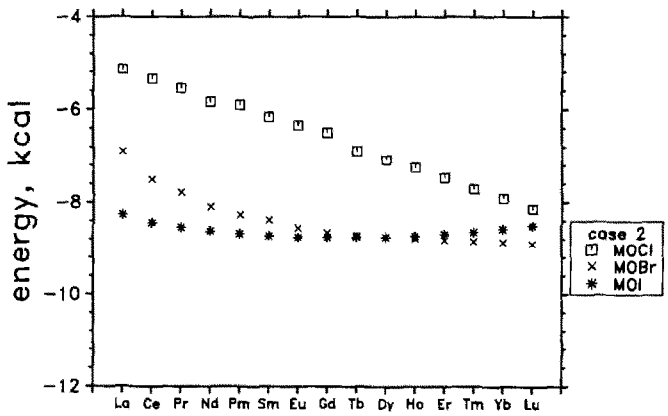

Fig. 38. The van der Waals energy of the second-nearest neighbor O–O bond, as calculated here using the lattice parameters labeled #2 in Table 2 and the D energy parameters listed in Table 4.

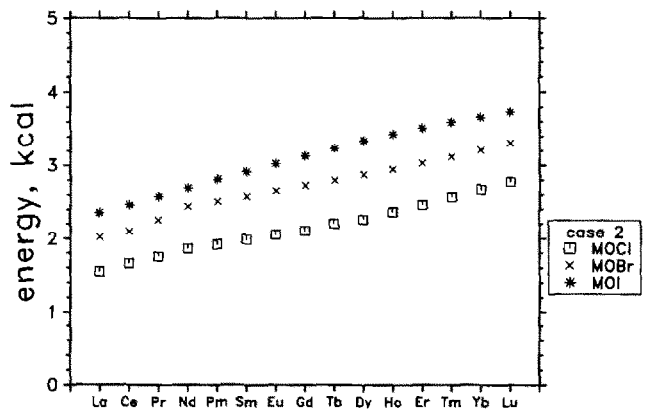

Fig. 39. The repulsive energy of the second-nearest neighbor O–O bond, as calculated here using the lattice parameters labeled #2 in Table 2 and the A and B energy parameters listed in Table 4.

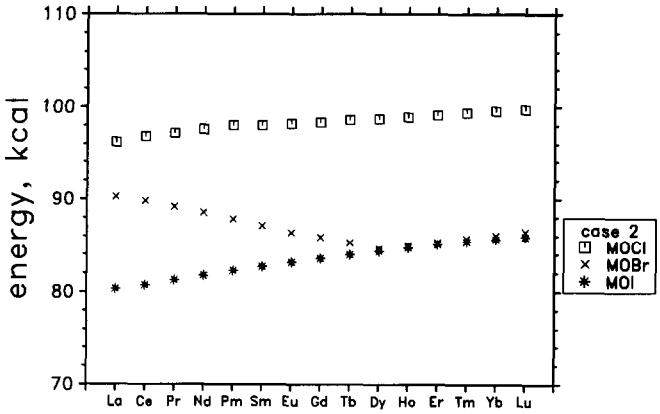

Fig. 40. The coulombic energy of the nearest neighbor X–X bond, as calculated here using the lattice parameters labeled #2 in Table 2.

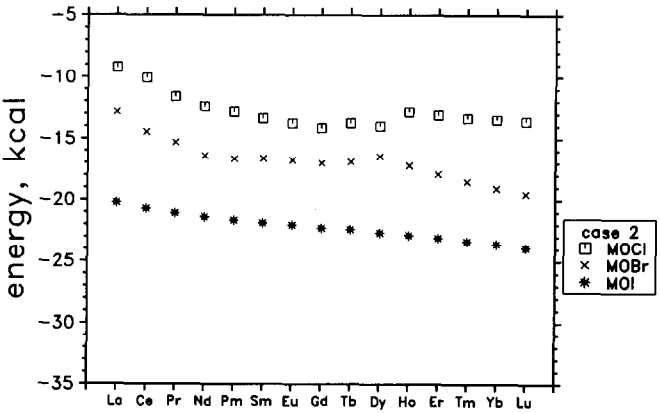

Fig. 41. The van der Waals energy of the nearest neighbor X–X bond, as calculated here using the lattice parameters labeled #2 in Table 2 and the *D* energy parameters listed in Table 4.

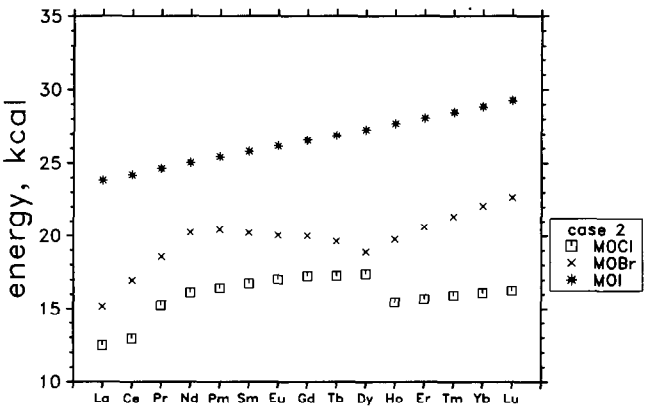

Fig. 42. The repulsive energy of the nearest neighbor X–X bond, as calculated here using the lattice parameters labeled #2 in Table 2 and the *A* and *B* energy parameters listed in Table 4.

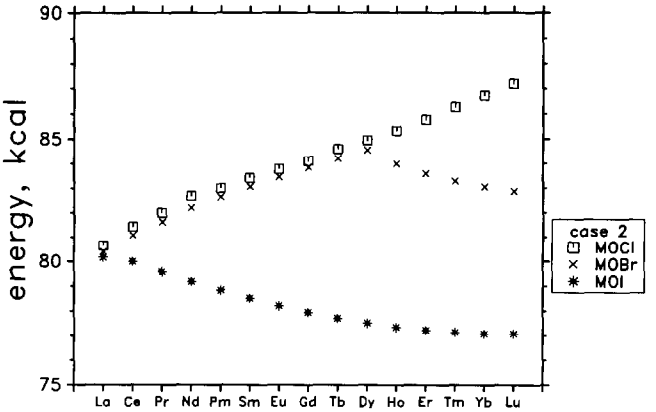

Fig. 43. The coulombic energy of the second-nearest neighbor X–X bond, as calculated here using the lattice parameters labeled #2 in Table 2.

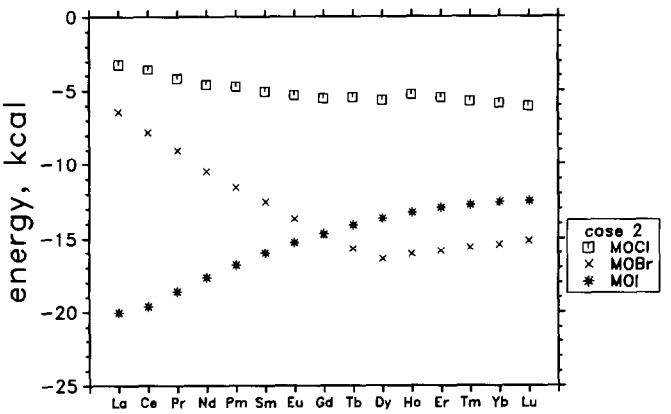

Fig. 44. The van der Waals energy of the second-nearest neighbor X–X bond, as calculated here using the lattice parameters labeled #2 in Table 2 and the *D* energy parameters listed in Table 4.

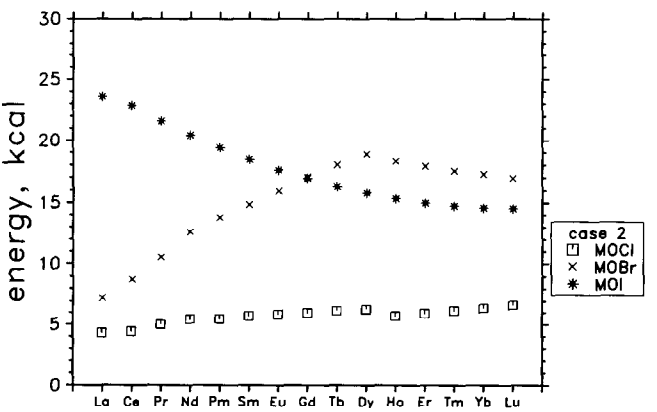

Fig. 45. The repulsive energy of the second-nearest neighbor X–X bond, as calculated here using the lattice parameters labeled #2 in Table 2 and the *A* and *B* energy parameters listed in Table 4.

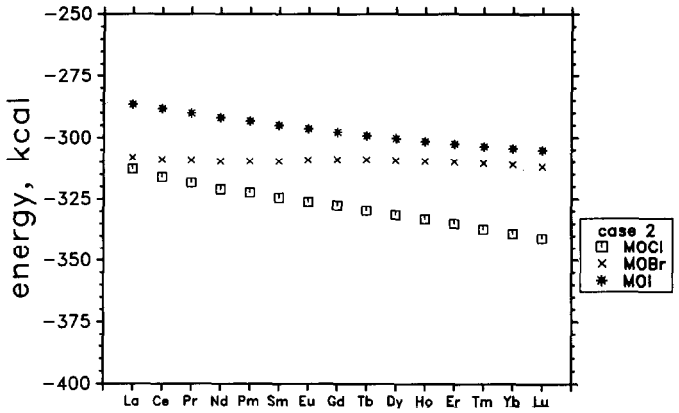

Fig. 46. The coulombic energy of the M–X bond between M and the four square-planar situated X neighbors, as calculated here using the lattice parameters labeled #2 in Table 2.

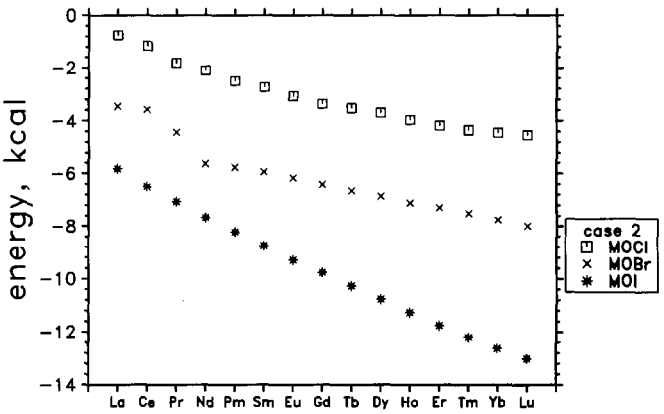

Fig. 47. The van der Waals energy of the M–X bond between M and the four square-planar situated X neighbors, as calculated here using the lattice parameters labeled #2 in Table 2 and the *D* energy parameters listed in Table 4.

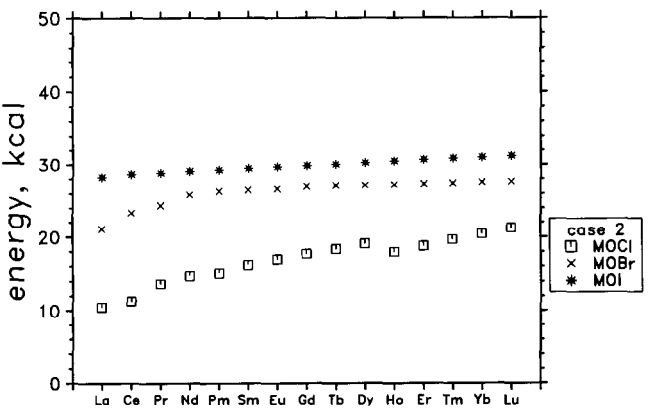

Fig. 48. The repulsive energy of the M–X bond between M and the four square-planar situated X neighbors, as calculated here using the lattice parameters labeled #2 in Table 2 and the *A* and *B* energy parameters listed in Table 4.

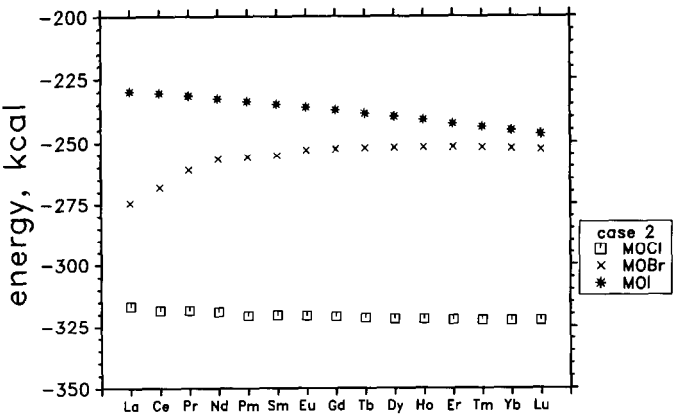

Fig. 49. The coulombic energy of the M–X bond between M and the closer of the two X neighbors displaced only along the z axis, as calculated here using the lattice parameters labeled #2 in Table 2.

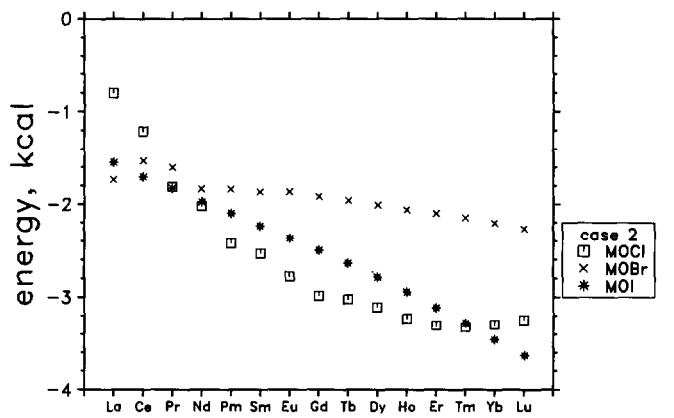

Fig. 50. The van der Waals energy of the M–X bond between M and the closer of the two X neighbors displaced only along the z axis, as calculated here using the lattice parameters labeled #2 in Table 2 and the D energy parameters listed in Table 4.

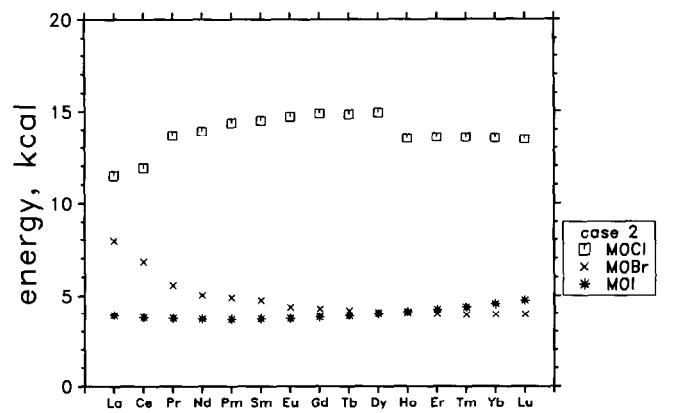

Fig. 51. The repulsive energy of the M–X bond between M and the closer of the two X neighbors displaced only along the z axis, as calculated here using the lattice parameters labeled #2 in Table 2 and the A and B energy parameters listed in Table 4.

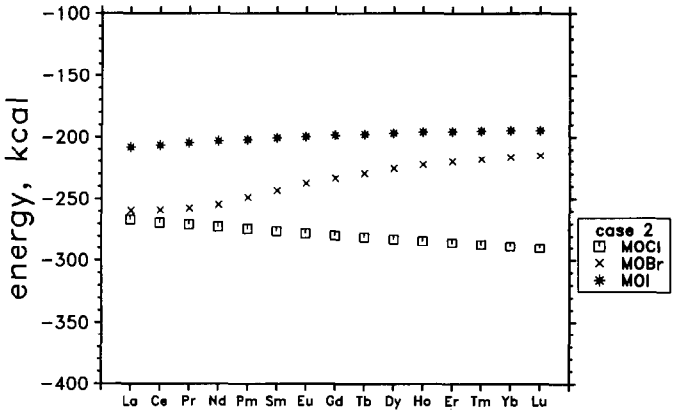

Fig. 52. The coulombic energy of the M–X bond between M and the further of the two X neighbors displaced only along the z axis, as calculated here using the lattice parameters labeled #2 in Table 2.

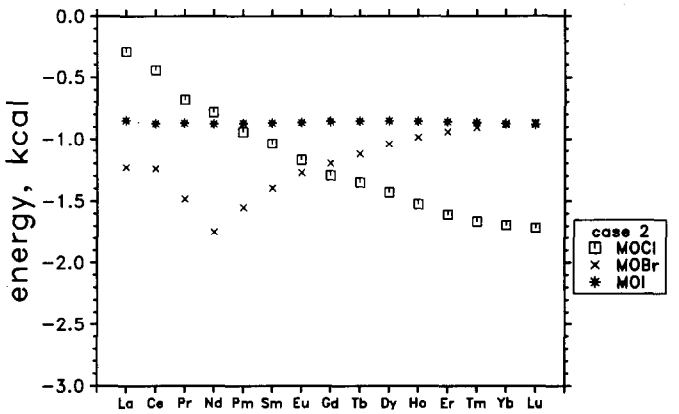

Fig. 53. The van der Waals energy of the M–X bond between M and the further of the two X neighbors displaced only along the z axis, as calculated here using the lattice parameters labeled #2 in Table 2 and the D energy parameters listed in Table 4.

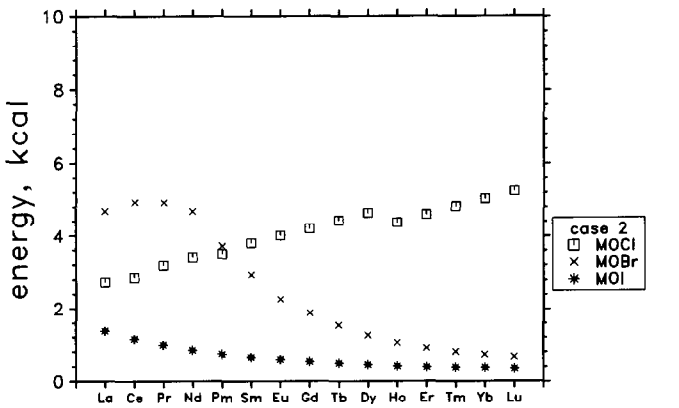

Fig. 54. The repulsive energy of the M–X bond between M and the further of the two X neighbors displaced only along the z axis, as calculated here using the lattice parameters labeled #2 in Table 2 and the A and B energy parameters listed in Table 4.

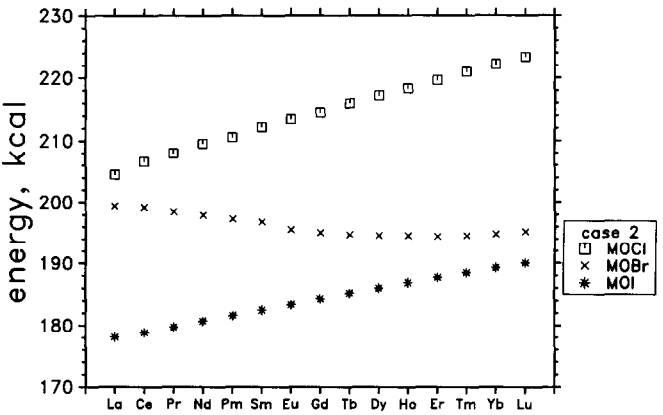

Fig. 55. The coulombic energy of the nearest neighbor O–X bond, as calculated here using the lattice parameters labeled #2 in Table 2.

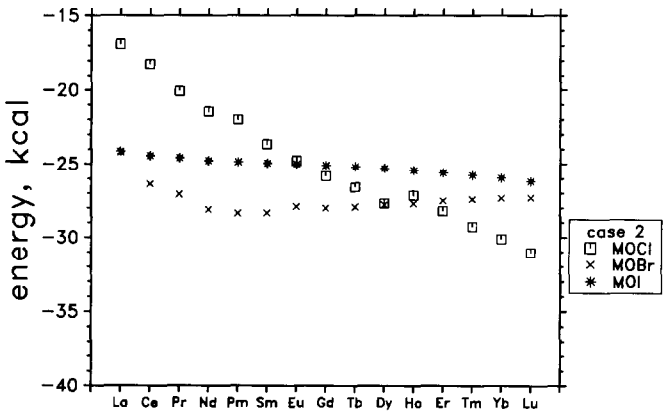

Fig. 56. The van der Waals energy of the nearest neighbor O–X bond as calculated here, using the lattice parameters labeled #2 in Table 2 and the *D* energy parameters listed in Table 4.

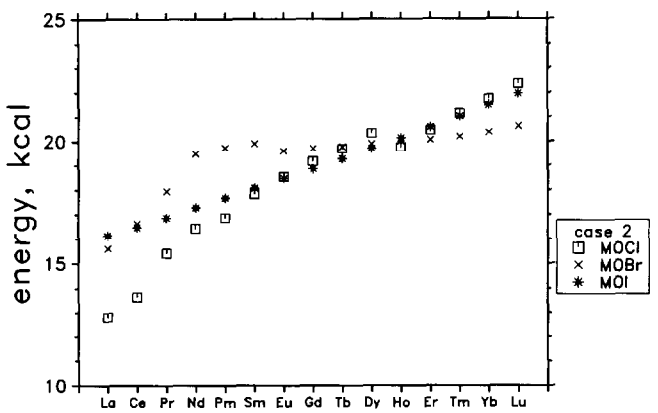

Fig. 57. The repulsive energy of the nearest neighbor O–X bond, as calculated here using the lattice parameters labeled #2 in Table 2 and the *A* and *B* energy parameters listed in Table 4.

DISCUSSION

Structures

The quantitative descriptions of the oxyhalide lattices adopted here are often unsupported by any experimental data, and, of even more concern, sometimes in contradiction with actual experimental data. Clearly there is a need for accurate determinations of all these lattice parameters and positional coordinates. However, as discussed above, the trends in the observed oxybromide data create some skepticism and some wariness with respect to the compositional purity of the measured samples. A likely possibility is contamination by hydroxyl ions.

Critique of the fit

The main difficulty with eqn. (2) is that the solutions found are not unique. We were forced into a prolonged search over the parameter space for sets that converge for all species, in the sense that the energies are as desired: that derivatives of the energy are zero with respect to changing a, c, u_x, and u_m. Once a set was found, however, a whole volume of the nine-dimensional parameter space for each species could be found. Within this volume of convergence, the value of some parameters can vary by more than a factor of two. Any point in parameter space for one species can be linked with points in parameter space for the other species to form many arbitary sets of allowed parameters. Only by imposing additional constraints (smoothness in the parameter values, the total energies and their components, and the individual bond energies and their components) does a single set emerge as the most probable.

Even the values for W_t themselves are not unique without appealing to smoothness. For example, the identical W_t values listed in Table 1 and obtained with the lattice description "#2" in Table 2, were also obtained using the lattice description labeled "#1" in Table 2, i.e. the lattice descriptions in the literature. However, the #1 description of the lattice yields parameters and bond energies that are much more poorly behaved. Within a narrow range, only the values of lattice parameters and energy parameters adopted here both satisfy the desired smoothness criteria and give acceptable W_t values.

The smoothness criterion is not completely realized, even for our adopted parameters. There are residual smoothness violations in the values plotted in Figs. 14, 15, 18, 19, 22, 25, 38, 44, 45, 50, 51, 53, 54, 56 and 57. It is possible that some set can be found, by further refinement, which reduces these residual irregularities. However, we are close to the optimum parameter set with respect to all of the smoothness criteria considered. Any improvement should not affect the derived enthalpies by more than a few kilocalories.

Need for an improved potential energy expression

The insensitivity of the predicted energy to lattice dimensions and positions, without the added criterion of smoothness, is one of the shortcomings of the potential energy function used here.

The function in eqn. (2) does not force the equilibrium positioning of all the ions in the unit cell. It does not demand P4/*nmm* to be the space group, i.e. it does not force all atoms to be placed at their equilibrium lattice positions, because it does not force W_t to be at its global minimum for this placement. The restriction to this space group is added separately by forcing the program to consider only excursions which preserve this space group. Only for changes in the a, c, u_x, and u_m parameters are the derivatives of eqn. (2) zero. The restriction of the angles in the structure to right angles is not demanded by eqn. (2) but only by the space group restriction.

An improved potential function should predict real frequencies for all vibrational modes in the crystal. Forcing the correct frequencies would eliminate much of the need to appeal to smoothness of behavior in the search for parameter values. In fact, however, eqn. (2) gives imaginary values to as many as half of the frequencies.

The term labeled "van der Waals" in eqn. (2) and varying as the inverse sixth power of interatomic distances is a hundred times larger than expected. It is actually mimicking the polarization terms which vary not as the sixth power but as the third through eighth powers, depending on their nature, and also the covalent contributions to the energy. Note that this van der Waals term is largest for the iodides, for which covalent contributions are expected to be greatest.

Equation (2), in addition to requiring smoothness as a separate criterion to obtain a unique solution, leads to little understanding of the transition of this crystal structure from three-dimensional to layered. There are long range coulombic forces, both attractive and repulsive, which are probably responsible for this behavior. However, there is no easy way of dissecting the lattice sum into what might be called the energy of the block and the energy of interactions between blocks. Even in the oxyiodides, for which the layered structure is quite evident, we could not separate the total energy into these two types during the time alloted us.

Dissociation enthalpies

Figure 12 shows the dissociation enthalpies obtained here. The trends shown are plausible, with all values positive, i.e. all oxyhalides are stable against breaking up into oxide and halide phases. The oxychlorides are shown as most stable, the oxyiodides least stable. There seems to be a

maximum in stability across the rare-earth series, and this maximum is systematically placed at lower atomic number as one goes from oxychloride through oxybromide to oxyiodide.

There is some slight scatter in the plot, at times by about 1 kcal mol^{-1}. This is in part due to the incompleteness in the smoothing of the oxide enthalpies of formation. It seems prudent to wait for some experimental corroboration of the greater changes that we invoked for Yb_2O_3 and Lu_2O_3 before proceeding with fractional kcal mol^{-1} smoothing adjustments. Also needed is some experimental determination which fixes the stabilities of a few oxyiodides and places a few oxybromides in this plot.

CONCLUSIONS

A set of enthalpies of formation of rare-earth oxychlorides, bromides, and iodides is provided. This set comes from a smoothing of the W_t values obtained through Born–Haber cycles from published oxychloride enthalpy values, and then an extrapolation to the oxybromides and oxyiodides. The adopted set was also required to give smooth behavior of the enthalpy of dissociation of the oxyhalide into oxide and halide phases.

The W_t values adopted here are supported by crystal energy calculations, using a potential function due to Busing. The cystallographic parameters and the Busing repulsive and van der Waals energy parameters were adjusted so as to provide smooth behavior in lattice dimensions, interatomic distances, total energies and their components, and individual bond energies and their components.

The enthalpy of dissociating oxyhalides into oxides and halides was plotted. The values plotted involve the published enthalpies of formation of the oxides. Some of these oxide enthalpies were found to give non-smooth W_t behavior across the rare-earth series, and their values were adjusted to give smoothness. With the smoothed values for the oxides, the dissociation enthalpies of the oxyhalides were found to vary smoothly and reasonably. All oxyhalides are stable with respect to breakup into oxide and halide. The oxychlorides are most stable, and the oxyiodides are least stable. The stability was found to have a maximum within the rare-earth series, with the maximum for the oxychloride placed at higher atomic number than the maximum for the oxyiodides and with the maximum for the oxybromide intermediate.

ACKNOWLEDGMENT

The authors are indebted to Dr. Charles Brecher for his helpful comments, especially those concerning our use of smoothing to gain uniqueness for the parameters of the lattice energy calculation.

REFERENCES

1 C.W. Struck and J.A. Baglio, An estimate of rare earth monohalide enthalpies of formation using the Rittner energy expression, High Temp. Sci., 30 (1991) 113–135.
2 C.W. Struck and J.A. Baglio, A potential energy expression for estimating rare-earth dihalide enthalpies of formation, High Temp. Sci., 31 (1991) 1–44.
3 C.W. Struck and J.A. Baglio, Estimates for the enthalpies of formation of rare-earth solid and gaseous trihalides, High Temp. Sci., 31 (1991) 209–237.
4 E.S. Rittner, Binding energy and dipole moment of alkali halide molecules, J. Chem. Phys., 19 (1951) 1030.
5 N.F.M. Henry and K. Lonsdale (Eds.), International Tables for X-Ray Crystallography, Kynoch Press for the International Union of Crystallography, Birmingham, U.K., 1952.
6 R.W.G. Wyckoff, Crystal Structures, Wiley, New York, 1965.
7 H. Bärnighausen, G. Brauer and N. Schultz, Darstellung und kristallstruktur der samarium-, europium, und ytterbium-oxidbromide LnOBr und Ln_3O_4Br, Z. Anorg. Allg. Chem., 338 (1965) 250–265.
8 W.F. McClune (Ed.), Powder Diffraction File, JCPDS, International Center for Diffraction Data, Swathmore, PA, 1991.
9 H. Häuseler and M. Jung, Single crystal growth and structure of LaOBr and SmOBr, Mater. Res. Bull., 21 (1986) 1291–1294.
10 M.W.M. Hisham and S.W. Benson, Thermochemistry of inorganic solids. 3. Enthalpies of formation of solid metal oxyhalide compounds, J. Phys. Chem., 90 (1986) 885.
11 F. Weigel and V. Wishnevsky, Wärmetönung und Gibbs energie der Reaktion $MCl_3(f) + H_2(g) = MOCl(f) + 2HCl(g)$ (M = Y, Tb), Chem. Ber., 106 (1973) 1976.
12 Yu.B. Patrikeev, G.I. Novikov and V.V. Badovskii, Thermal dissociation of scandium, ytrium, and lanthanum oxide chlorides, Russ. J. Phys. Chem., 47 (1973) 284.
13 L.B. Pankratz, Thermodynamic properties of elements and oxides, Tech. Report Bulletin 672, United States Department of the Interior, Bureau of Mines, 1982.
14 W.R. Busing, WMIN, a computer program to model molecules and crystals in terms of potential energy functions, Tech. Report ONLR-5747, Oak Ridge National Laboratory, Oak Ridge, TN 37830, 1981.
15 W.R. Busing, An interpretation of the structures of alkaline earth chlorides in terms of interionic forces, Proc. Symp. Intermolecular Forces and Packing in Crystals, Trans. Am. Crystallogr. Assoc., 6 (1970) 57–72.